Chapter 4

Gegenbauer wavelet operational matrix method for solving variable order non-linear reaction-diffusion and Galilei invariant advection-diffusion equations

4.1 Introduction

Samko and Ross [70] have investigated fractional operator when the order is variable during many physical processes. This generalization of fractional derivative to be a non-constant depending on time and space is very interesting. This approach of variable order fractional calculus has numerous applications in physics, mechanics, control and signal processing [71, 72, 73]. There are many definitions of variable order

fractional derivative and integration. The variable order operators have too complex kernel for having a variable exponent. So, to find numerical solution of variable order fractional differential equation(VOFDE) is a little bit tough task as compared to constant order differential equation. In article [74], a consistent approximation is used to solve VOFDE. A finite difference scheme to find solution of VOFDE and convergence analysis is used in article [75]. Some latest and updated methods are discovered to find the numerical solution of VOFDE viz., finite difference method[23, 24], B-linear spline method [76], Cubic spline method [77, 78], Integro quadratic spline interpolations [79, 80] and spectral method [81]. Analytic solution of variable order differential equation is given in article [82]. Variable-order fractional Laplacian equation with variable growth has been solved in article [83]. In article [84], spectral collocation method is proposed to solve some linear and nonlinear VOFPDE. An accurate discretization technique has been developed in [20] to solve variable-order fractional reaction-diffusion problems.

Reaction-diffusion process has been investigated from a long time. In the process of reaction- diffusion, reacting molecules are used to move through space due to diffusion. This definition excludes other modes of transports as convection, drift those may arise due to presence of externally imposed fields.

When a reaction occurs within an element of space, molecules can be created or consumed. These events are added to the diffusion equation and lead to reaction-diffusion equation of the form

$$\frac{\partial c}{\partial t} = D\nabla^2 c + R(c,t), \tag{4.1}$$

where $R(c,t)$ denotes reaction term at time t. The extension of the reaction-diffusion equation in fractional order system can be found in the articles [85, 86, 87, 88]. In nature many of the beautiful systems in biology, physics,chemistry, and physiology

can be described by reaction diffusion equations. For example, the distribution and organization of vegetation-like bushes in arid ecosystems [89], the stripes and spots on fish [90], snakes [91] and the skin or fur of mammals [92] have been studied by the standing waves which are produced by reaction-diffusion equations.

The advection diffusion equation is a combination of diffusion and convection. The transport of material by a known velocity field can be described by the reaction-advection diffusion equation(RADE). The general form of this equation is

$$\frac{\partial u(x,t)}{\partial t} = \nabla.(C\nabla u) - \nabla.(\nu u) + R,$$

where $u(x,t)$ is variable representing concentration of mass transfer, temperature of heat transfer. C is diffusion coefficient and ν is the velocity of fluid flow as a function of time and location.

The fractional order reaction advection-diffusion equation (RADE) is generalized version of classical RADE. Many physical phenomena like transport dynamics in complex system, glassy and porous media, geological and geophysical processes can be modeled by advection-diffusion equation. Einstein's theory of Brownian motions reveals that the mean square displacement of a particle moving randomly is proportional to time. Thus in the fundamental solution of the integer order transport equation the probability density function governs the Brownian motion will be Gaussian type whose mean square displacement is $< X^2(t) > \sim t$ and if the integer order transport equation is extended to the time-fractional order system then phenomena of anomalous diffusion are observed. Therefore after the advancement of fractional calculus, it is seen that the mean square displacement for an anomalous diffusion equation having time fractional derivative grows slowly with time. For the simple fractional order diffusion equation $\frac{\partial^\alpha u}{\partial t^\alpha} = \frac{\partial^2 u}{\partial x^2}$, the mean square displacement is $X^2(t) \sim t^\alpha$ where α is anomalous diffusion exponent. An important characteristic of

this evolution equation is that it generates the fractional Brownian motion, a generalization Brownian motion. Thus if the integer order derivative is replaced by the fractional one, it changes the fundamental concept of time and the concept of evolution in the foundations of physics. The fractional order derivative has a physical meaning related to the statistics of waiting times according to the Montroll-Weiss theory. It can also be shown that for fractional order reaction advection diffusion equation (RADE), the mean square displacement will be $< X^2(t) > \sim t^{\frac{3\alpha}{2}}, 0 < \alpha < 1$ and thus it can be said that the transportation equation of the form of RADE follows the evolutionary process.

4.2 Preliminaries

Here, few definitions and important properties of fractional calculus have been introduced. In literature, definitions of two types of variable order derivative have been introduced. These two definitions are named as variable order derivative type $1(V1)$ and variable order derivative type $2(V2)$. Here the definitions suggested in [74, 78] have been used.

4.2.1 Variable-order derivatives of Type $1(V1)$ and Type $2(V2)$

From this definition of Type $1(V1)$ derivative, it can be shown that memory effect of a given system is changed with time and can be determined by its current state. So, variable order definition is useful to characterize variable memory effect of the system. Type 1 (V1) form of variable order operator is useful to depict properly different real world diffusion processes. From the definition, it can be easily seen

that the variable order fractional derivative follows the linearity property as

$$ {}_0D_t^{\vartheta(t)}(c_1 f(x,t) + c_2 g(x,t)) = c_{10}D_t^{\vartheta(t)} f(x,t) + c_{20}D_t^{\vartheta(t)} g(x,t). \tag{4.2} $$

It has the following useful property as

$$ {}_0D_t^{\vartheta(t)} t^m = \begin{cases} \dfrac{\Gamma(m+1)}{\Gamma(m-\vartheta(t)+1)} t^{m-\vartheta(t)}, & q \leq m, \\ 0, & otheerwise. \end{cases} \tag{4.3} $$

In article [93], it is shown that fractional derivative shows the long memory effect of a system and memory effect is reduced as the order approaches to integer order. The consequences represent that memory effect depicted by V1 type operator model changes with fast rate as compared to the model containing V2 type operator model. Since model of V2 type contains memory of its history, it prevents the system behavior from changing sharply.

4.2.2 Gegenbauer polynomial and Gegenbauer wavelet

The Gegenbauer polynomials also known as ultra spherical harmonics polynomials denoted by $G_\lambda^n(x)$, for $\lambda > \frac{-1}{2}$ satisfy the following singular sturm-Liouville equation on $[-1, 1]$ as

$$ \frac{d}{dy}[(1-y^2)^{\lambda+\frac{1}{2}} \frac{d}{dy} G_\lambda^n(y)] + n(n+2\lambda)(1-y^2)^{\lambda-\frac{1}{2}} G_\lambda^n(y) = 0. \tag{4.4} $$

These polynomials can also be derived by following recurrence relations

$$G_\lambda^0(y) = 0, G_\lambda^1(y) = 2\lambda y, \tag{4.5}$$

$$G_\lambda^{n+1}(y) = \frac{1}{n+1}[2y(\lambda+n)G_\lambda^n(y) - (2\lambda+n-1)G_\lambda^{n-1}(y)]. \tag{4.6}$$

The Rodrigue's formula to compute the Gegenbauer polynomials is given by

$$G_\lambda^n(y) = (\frac{-1}{2})^n \frac{\Gamma(\lambda+\frac{1}{2})\Gamma(n+2\lambda)}{n!\Gamma(2\lambda)\Gamma(n+\lambda+\frac{1}{2})}(1-y^2)^{-\lambda+\frac{1}{2}}\frac{d^n}{dy^n}(1-y^2)^{n+\lambda-\frac{1}{2}}. \tag{4.7}$$

The Gegenbauer polynomials are orthogonal on the interval$[-1,1]$ with respect to the weight function $w(x) = (1-y^2)^{\lambda-\frac{1}{2}}$.

$$\int_{-1}^{1}(1-y^2)^{\lambda-\frac{1}{2}}G_\lambda^m(y)G_\lambda^n(y)dy = L_m^\lambda \delta_{mn}, \lambda > \frac{-1}{2}, \tag{4.8}$$

where $L_m^\lambda = \frac{\pi 2^{1-2\lambda}\Gamma(m+2\lambda)}{m!(m+\lambda)(\Gamma\lambda)^2}$ is normalizing factor and δ is the Kronecker delta function. This following inequality holds for Gegenbauer polynomials:

$$|G_\lambda^n(\cos\theta)|(\sin\theta)^\lambda < \frac{\Gamma(n+\frac{3\lambda}{2})2^{1-\lambda}}{\Gamma(\lambda)\Gamma(1+n+\frac{\lambda}{2})}, 0 \le \theta \le \pi. \tag{4.9}$$

Another recurrence relation with integration is

$$\int G_\lambda^n(x)w(x)dx = \frac{-2\lambda(1-x^2)^{\frac{1}{2}+\lambda}}{n(n+2\lambda)}G_{\lambda+1}^{n-1}(x). \tag{4.10}$$

Gegenbauer wavelet can be defined on $[0,1]$ by

$$\psi_{n,m}^\lambda(x) = \begin{cases} \frac{1}{\sqrt{L_m^\lambda}}2^{\frac{k}{2}}G_\lambda^m(2^k x - \hat{n}), & \frac{\hat{n}-1}{2^k} < x < \frac{\hat{n}+1}{2^k} \\ 0 & otherwise, \end{cases} \tag{4.11}$$

where $k = 1, \cdots$, $n = 1, \cdots 2^{k-1}$, $\hat{n} = 2n-1$ is translation parameter, m in the order of Gegenbauer wavelet. For each λ a different family of wavelets can be generated. Putting $\lambda = 0$ and $\lambda = 1$, Chebyshev wavelets of first and second kinds are obtained, respectively. Putting $\lambda = \frac{1}{2}$, the family of Legendre wavelets is obtained.

4.3 Function Approximation

Gegenbauer wavelet can be used to expand any function $f(x)$ defined over $[0, 1]$ as

$$f(x) = \sum_{n=0}^{\infty} \sum_{m=0}^{\infty} c_{nm} \psi_{n,m}^{\lambda}(x), \tag{4.12}$$

where $c_{pq} = \int_0^1 f(x) \psi_{n,m}^{\lambda}(x) w_n^{\lambda}(x) dx$.
Here $w_n^{\lambda}(x) = (1 - (2^k x(2n-1))^2)^{\lambda - 1/2}$ is the weight function. The truncate form of the above infinite series is

$$f(x) = \sum_{n=0}^{2^{k-1}} \sum_{m=0}^{M-1} c_{nm} \psi_{n,m}^{\lambda}(x) = C^T \Psi(x), \tag{4.13}$$

where C^T is row vector of unknown coefficient and $\Psi(x)$ is the Gegenbauer column vector of order $2^{k-1}M$. Now rewrite this equation in matrix form as

$$f(x) = \sum_{k=0}^{\hat{m}} c_k \psi_k^{\lambda}(x) = C^T \Psi(x), \tag{4.14}$$

where $\hat{m} = 2^{k-1}M$ and $k = Mn + m + 1$.
Similarly, an arbitrary function of two variables can be expanded in terms of Gegenbauer wavelet as

$$f(x,t) = \sum_{k=0}^{\hat{m}} \sum_{l=0}^{\hat{m}} c_{kl} \psi_k^{\lambda}(x) \psi_l^{\lambda}(t) = \Psi^T(x) V \Psi(t), \tag{4.15}$$

where $V = [c_{ij}]$ and $c_{ij} = \int_0^1 \int_0^1 f(x,t)\psi_i^\lambda(x)\psi_j^\lambda(t)w_n^\lambda(x)w_n^\lambda(t)dxdt$.

4.4 Error bound and stability analysis

In this section, a discussion on error analysis, convergence of Gegenbauer wavelet and derive an upper bound for the truncation error is taken place.

Theorem 2: A function $g(x) \in L^2[0,1]$ can be approximated as an infinite series of Gegenbauer wavelets. This series will converge uniformly to $g(x)$, with given condition $|g''(x)| \leq M$. Moreover, expansion coefficient given in equation (4.12) satisfies the inequality

$$|c_{nm}| < \frac{4M(1+\lambda)^2(1+m+\lambda)^2}{n^{\frac{5}{2}}(m-2)^4}, \forall n \geq 1, m > 2. \tag{4.16}$$

Proof: With the help of definition given in equation (4.11) and by the properties of inner product, the coefficients c_{nm} can be written as

$$c_{nm} = \frac{1}{\sqrt{L_m^\lambda}} 2^{\frac{k}{2}} \int_{\frac{n-1}{2^{k-1}}}^{\frac{n}{2^{k-1}}} g(x) G_\lambda^m(2^k x - 2n + 1) w(2^k x - n) dx. \tag{4.17}$$

Integrating by parts of right hand side of above equation along with property (4.11) of Gegenbauer wavelets

$$c_{nm} = \frac{\lambda 2^{\frac{6-k}{2}}}{m(m+2\lambda)\sqrt{L_m^\lambda}} \int_{\frac{n-1}{2^{k-1}}}^{\frac{n}{2^{k-1}}} g'(x) G_{\lambda-1}^{m-1}(2^k x - 2n + 1) \\ (2^k x - n)(1 + n - 2^k t) w(2^k x - n) dx. \tag{4.18}$$

Again integrating by parts and substituting $2^k t - 2n + 1 = \cos\theta$, we can rewrite the above equation as

$$c_{nm} = \frac{2^{-2\lambda-\frac{5k-5}{2}}(\lambda)_2\sqrt{2}}{(m-1)_2(m-1+2\lambda)_2\sqrt{L_m^\lambda}} \int_0^\pi g''(\frac{\cos\theta+2n+1}{2^k}) G_{\lambda-2}^{m-2}(\sin\theta)^{2\lambda+4}\cos\theta d\theta. \tag{4.19}$$

Now, considering inequality (4.9) and assuming $|g''(x)| \leq M$, we get

$$\begin{aligned} |c_{nm}| \leq & \frac{2^{-2\lambda-\frac{5k-5}{2}}|(\lambda)(\lambda+1)|\sqrt{2}}{(m-1)_2(m-1+2\lambda)_2|\sqrt{L_m^\lambda}|} \times \int_0^\pi |g''(\frac{\cos\theta+2n+1}{2^k})||G_{\lambda-2}^{m-2}(\sin\theta)^{2\lambda+4}\cos\theta|d\theta. \\ < & \frac{M2^{-2\lambda-\frac{5k-5}{2}}|(\lambda)(\lambda+1)|\sqrt{2}}{(m-1)_2(m-1+2\lambda)_2|\sqrt{L_m^\lambda}|} \times \int_0^\pi |G_{\lambda-2}^{m-2}(\sin\theta)^{2\lambda+4}\cos\theta|d\theta. \end{aligned} \tag{4.20}$$

Putting the value of $\sqrt{L_m^\lambda}$, the following value is obtained as

$$|c_{nm}| < \frac{4M(\lambda+1+m)^2(1+\lambda)^2}{(m-2)^4 n^{\frac{5}{2}}}, \tag{4.21}$$

which completes the proof of theorem.

Next for the error bound let us consider a function $u(x,t) \in C^M[0,1]$ where $(x,t) \in [0,1]\times[0,1]$. Consider

$$\Theta_M = Span\{G_i^\lambda G_j^\lambda, i,j = 0,1\cdots M-1\}. \tag{4.22}$$

Assuming $\tilde{u}(x,t) \in \Theta_M$ is better approximation of $u(x,t)$, we obtain

$$\|u(x,t) - \tilde{u}(x,t)\| \leq \|u(x,t) - w(x,t)\|, \forall w(x,t) \in \Theta_M. \tag{4.23}$$

Now following the procedure as given in [94, 95], we get

$$u(x,t)-w(x,t)=\frac{1}{M!}\frac{\partial^M u(\varsigma,t)}{\partial x^M}\prod_{i=1}^{M-1}(x-x_i)+\frac{1}{M!}\frac{\partial^M u(x,\tau)}{\partial t^M}\prod_{i=1}^{M-1}(t-t_j)$$
$$-\frac{1}{(M!)^2}\frac{\partial^{2M} u(\varsigma',\tau')}{\partial x^M\partial t^M}\prod_{j=1}^{M-1}(t-t_j)\prod_{i=1}^{M-1}(x-x_i), \tag{4.24}$$

where ς, τ, ς',$\tau' \in [0,1]$, x_i and t_j are roots of G_M^{λ}.

Now,

$$\|u(x,t)-w(x,t)\| \leq \frac{1}{M!}\max_{(x,t)}\left|\frac{\partial^M u}{\partial x^M}\right|\left\|\prod_{i=1}^{M-1}(x-x_i)\right\|+\frac{1}{M!}\max_{(x,t)}\left|\frac{\partial^M u}{\partial t^M}\right|\left\|\prod_{i=1}^{M-1}(t-t_j)\right\|$$
$$-\frac{1}{(M!)^2}\max_{(x,t)}\left|\frac{\partial^{2M} u}{\partial x^M\partial t^M}\right|\left\|\prod_{j=1}^{M-1}(t-t_j)\right\|\left\|\prod_{i=1}^{M-1}(x-x_i)\right\|. \tag{4.25}$$

As $u(x,t)\in C^M[0,1]$, then there exist N_1, N_2 and N_3 such that

$$\max_{(x,t)}\left|\frac{\partial^M u}{\partial x^M}\right|\leq N_1, \max_{(x,t)}\left|\frac{\partial^M u}{\partial t^M}\right|\leq N_2, \max_{(x,t)}\left|\frac{\partial^{2M} u}{\partial x^M\partial t^M}\right|\leq N_3. \tag{4.26}$$

By minimizing the factor $\left\|\prod_{i=1}^{M-1}(x-x_i)\right\|$, we obtain

$$\|u(x,t)-\tilde{u}(x,t)\|\leq N_3\frac{4}{(M!)^2 4^{2M}}+(N_1+N_2)\frac{4}{(M!)4^M}=H(N_1,N_2,N_3,M). \tag{4.27}$$

Thus an upper bound has been derived for the absolute error with respect to Gegenbauer polynomial.

Theorem 3: Let $u(x,t)\in C^M[0,1]$ defined on domain $(x,t)\in[0,1]\times[0,1]$ with

$$\max_{(x,t)}\left|\frac{\partial^M u}{\partial x^M}\right|\leq N_1, \max_{(x,t)}\left|\frac{\partial^M u}{\partial t^M}\right|\leq N_2, \max_{(x,t)}\left|\frac{\partial^{2M} u}{\partial x^M\partial t^M}\right|\leq N_3, \tag{4.28}$$

where N_1, N_2 and N_3 are constants. If $u(x,t)$ has Gegenbauer wavelet expansion as $\Psi^T(x).V.\Psi(t)$ then error bound is given by

$$\|u(x,t) - \Psi^T(x)V\Psi(t)\| \leq H(N_1,N_2,N_3,M)\frac{\sqrt{\pi}}{2^{\frac{k+1}{2}}}\frac{\Gamma(\frac{1}{2}+\lambda)}{\Gamma(1+\lambda)}. \tag{4.29}$$

Proof: By the orthogonality condition of Gegenbauer wavelet

$$\|u(x,t) - \Psi^T(x)V\Psi(t)\|^2 = \int_0^1\int_0^1 w_n^\lambda(x)w_n^\lambda(t)(u(x,t)-\Psi^T(x)V\Psi(t))^2dxdt. \tag{4.30}$$

Since the domain has been divided into 2^{2k} sub domains so the following expression is obtained as

$$\begin{aligned}\|u(x,t) - \Psi^T(x)V\Psi(t)\|^2 &= \sum_{n=0}^{2^{k-1}}\sum_{n'=0}^{2^{k-1}}\int_{\frac{n-1}{2^{k-1}}}^{\frac{n}{2^{k-1}}}\int_{\frac{n'-1}{2^{k-1}}}^{\frac{n'}{2^{k-1}}} w_n^\lambda(x)w_n^\lambda(t)(u(x,t)-\Psi^T(x)V\Psi(t))^2dxdt \\ &\leq \sum_{n=0}^{2^{k-1}}\sum_{n'=0}^{2^{k-1}}\int_{\frac{n-1}{2^{k-1}}}^{\frac{n}{2^{k-1}}}\int_{\frac{n'-1}{2^{k-1}}}^{\frac{n'}{2^{k-1}}} w_n^\lambda(x)w_n^\lambda(t)\big(u(x,t)-\tilde{u}(x,t)\big)^2dxdt,\end{aligned} \tag{4.31}$$

where $\tilde{u}(x,t)$ satisfies the error bound given in equation (4.28). Now it can be derived as

$$\begin{aligned}\|u(x,t) - \Psi^T(x)V\Psi(t)\|^2 &\leq (H(N_1,N_2,N_3,M))^2\sum_{n=0}^{2^{k-1}}\sum_{n'=0}^{2^{k-1}}\int_{\frac{n-1}{2^{k-1}}}^{\frac{n}{2^{k-1}}}\int_{\frac{n'-1}{2^{k-1}}}^{\frac{n'}{2^{k-1}}} w_n^\lambda(x)w_n^\lambda(t)dxdt \\ &\leq (H(N_1,N_2,N_3,M))^2\frac{\pi}{2^{k+1}}\frac{\Gamma(\frac{1}{2}+\lambda)^2}{\Gamma(1+\lambda)^2},\end{aligned} \tag{4.32}$$

which completes the proof of the theorem.

4.5 Operational matrix of derivative

Therorem 4: If $\Psi(t)$ denotes the Gegenbauer wavelet, then derivative of $\Psi(t)$ can be written as

$$\frac{d}{dx}\Psi(t) = \overline{D}\Psi(t), \tag{4.33}$$

where $\overline{D}$ is an operational matrix of order $2^{k-1}M$ which can be defined as

$$\overline{D} = \begin{bmatrix} \theta & 0 & 0 & \cdots & 0 \\ 0 & \theta & 0 & \cdots & 0 \\ 0 & 0 & \theta & \cdots & 0 \\ \vdots & \vdots & \cdots & \vdots & \\ 0 & 0 & 0 & \cdots & \theta \end{bmatrix},$$

where θ is a matrix of order $M \times M$ having (l, m)th elements defined as

$$\theta_{h,k} = \begin{cases} \frac{2^{m+1}(m+\lambda-1)}{\sqrt{\frac{(m-1+\lambda)\Gamma(m)\Gamma(h-1+2\lambda)}{(l-1+\lambda)\Gamma(l)\Gamma(m-1+2\lambda)}}}, & l = 2, \cdots, M, k = 1, \cdots, l-1 and (l+m) odd \\ 0, & otherwise. \end{cases} \tag{4.34}$$

In general, n-times derivative of vector $\Psi(x)$ is expressed by

$$\frac{d^n}{dx^n}\Psi(x) = \overline{D}^n\Psi(x), \tag{4.35}$$

where D^n is the n-th power of $\overline{D}$.

4.5.1 Gegenbauer wavelet operational matrix of variable-order fractional derivative

Type 1 fractional derivative of variable order $(q-1) < \gamma(x,t) \leq q$ of a Gegenbauer vector $\Psi(t)$ can be defined as

$$ {}_0D_t^{\gamma(x,t)}\Psi(t) \simeq Q_t^{\gamma(x,t)}\Psi(t), \tag{4.36}$$

where $Q_t^{\gamma(x,t)}$ is an $\hat{m}\times\hat{m}$ operational matrix of variable order for Gegenbauer wavelet. To derive explicit form of this matrix, another family of piecewise functions is introduced, which are defined on $[0,1]$ as

$$\omega_{nm}(t) = \begin{cases} t^m, & t \in [\frac{n}{2^k}, \frac{n+1}{2^k}], \\ 0, & otherwise, \end{cases} \tag{4.37}$$

for $n = 0, 1, \cdots, 2^{k-1}$, $m = 0, 1, \cdots, M-1$. An $\hat{m}$ set of these non-normalized function can be expressed as

$$\Omega(t) = [\omega_1(t), \omega_2(t), \cdots, \omega_{\hat{m}}(t)]^T, \tag{4.38}$$

where $\omega_i(t) = \omega_{nm}(t)$ and index i can be determined by $i = Mn + m + 1$. If $\Omega(t)$ and $\Psi(t)$ are vectors defined in equations (4.38) and (4.13) then

$$\Omega(t) = P\Psi(t), \tag{4.39}$$

where $P = [p_{ij}]$ is $\hat{m} \times \hat{m}$ order matrix whose elements are determined by $p_{ij} =< \omega_i(t), \psi_j(t) >$.

Lemma. Let $\Omega(t)$ be the vector defined in equation (4.38) and $(q-1) < \gamma(x,t) \leq q$ be a positive function defined on $[0,1]$. Then V1 type fractional derivative of variable

order $\gamma(x,t)$ of $\omega_{nm}(t)$ can be expressed as

$$ {}_0D_t^{\gamma(x,t)}\omega_{nm}(t) = \begin{cases} \frac{m!}{\Gamma(m-\gamma(x,t)+1)}t^{m-\gamma(x,t)}, & m = q, q+1, \cdots, M-1, t \in [\frac{n}{2^k}, \frac{n+1}{2^k}], \\ 0, & otherwise. \end{cases} \tag{4.40} $$

Proof: Using relation (4.3), it can be proved easily.

Theorem 5: Let us assume $\Omega(t)$ be the vector which is defined in equation (4.38) and $(q-1) < \gamma(x,t) \leq q$ is a positive function defined over $[0,1]$. Then fractional derivative of variable order of Type 1 of $\Omega(t)$ can be defined as

$$ {}_0D_t^{\gamma(x,t)}\Omega(t) = V_t^{\gamma(x,t)}\Omega(t), \tag{4.41} $$

where $V_t^{\gamma(x,t)}$ is a matrix of order $\hat{m} \times \hat{m}$, which can be defined by

$$ V_t^{\gamma(x,t)} = \begin{bmatrix} S_t^{\gamma(x,t)} & 0 & 0 & \cdots & 0 \\ 0 & S_t^{\gamma(x,t)} & 0 & \cdots & 0 \\ 0 & 0 & S_t^{\gamma(x,t)} & \cdots & 0 \\ \vdots & \vdots & \cdots & \vdots & \\ 0 & 0 & 0 & \cdots & S_t^{\gamma(x,t)} \end{bmatrix}, $$

where $S_t^{\gamma(x,t)}$ is an $M \times M$ matrix given by

$$S_t^{\gamma(x,t)} = t^{-\gamma(x,t)} \begin{bmatrix} 0 & 0 & \cdots & 0 & \cdots & 0 & \cdots & 0 \\ \vdots & \vdots & \cdots & \vdots & \cdots & 0 & \cdots & 0 \\ 0 & 0 & \cdots & 0 & & & & \\ 0 & \cdots & 0 & \frac{q!}{\Gamma(q-\gamma(x,t)+1)} & 0 & 0 & \cdots & 0 \\ 0 & \cdots & 0 & 0 & \frac{(q+1)!}{\Gamma(q-\gamma(x,t)+2)} & 0 & \cdots & 0 \\ \vdots & \vdots & \cdots & \vdots & & & & \\ \vdots & \vdots & \vdots & \vdots & \vdots & \vdots & \frac{(M-1)!}{\Gamma(M-\gamma(x,t)+2)} & 0 \\ 0 & 0 & 0 & 0 & \cdots & 0 & 0 & \frac{M!}{\Gamma(M-\gamma(x,t)+1)} \end{bmatrix}.$$

Proof: By using above lemma the proof becomes very straight forward.

Theorem 6: Let $\Psi(t)$ be the Gegenbauer vector defined in equation (4.13) and $(q-1) < \gamma(x,t) \leq q$ be a positive function defined on $[0,1]$. Then the variable order fractional derivative of $\Psi(t)$ is given as

$$ {}_0D_t^{\gamma(x,t)}\Psi(t) = Q_t^{\gamma(x,t)}\Psi(t) = (P^{-1}V_t^{\gamma(x,t)}P)\Psi(t). \tag{4.42}$$

Proof: By considering equation (4.38), we get

$$\Psi(t) = P^{-1}\Omega(t), \tag{4.43}$$

and thus

$$ {}_0D_t^{\gamma(x,t)}\Psi(t) = P^{-1}\,{}_0D_t^{\gamma(x,t)}\Omega(t) = P^{-1}V_t^{\gamma(x,t)}\Omega(t) = (P^{-1}V_t^{\gamma(x,t)}P)\Psi(t), \tag{4.44}$$

which shows the proof of theorem.

4.6 Proposed model

In past decades, constant order fractional model of diffusion equation has been considered and achieved success in many fields. For more complicated and realistic stochastic diffusion process [96] it became clear that more theoretical and numerical studies are needed. Many problems of physical, biological and physiological diffusion phenomena are not equipped to characterize by CO fractional diffusion equation. These phenomena are complex to analysis and diffusion behaviors are changed with time evolution, space variation or on system parameters. Such kind of phenomena exist in various fields like as plasma physics, biophysics, protein dynamics [97] and econophysics [98]. In several diffusion processes diffusion rate decreases with the increasing in time from normal diffusion to sub diffusion. So, to characterize for this type of diffusion phenomena time dependent variable order model is a good choice. Diffusion in complex medium is a fast developing issue of research. Constant order diffusion model can describe diffusion phenomena in homogeneous medium. But in complex medium, the heterogeneities of the medium cause variations of permeability in different spatial positions. For this type of situation, variable order model with space dependent is best approach by which location dependent diffusion process can be explained. In addition, studying diffusion process in a porous media when external field or medium structure vary with time then constant order model can not used to characterize this phenomenon. When the problem of groundwater problem is considered in a medium through which flow occurs is heterogeneous and changes with time, VO reaction diffusion model is suggested. In this chapter as a first model, time variable order reaction diffusion equation is chosen given by the following equation

$$ {}_0D_t^{\gamma(x,t)}u(x,t) =_0 D_x^{\mu(x,t)}u(x,t) + \kappa(u(x,t)) + f(x,t), \tag{4.45}$$

with initial and boundary conditions as

$$\begin{aligned} u(x,0) &= f_1(x), \\ u(0,t) &= g_1(t), \\ u(1,t) &= g_2(t), \end{aligned} \tag{4.46}$$

where $\kappa(u(x,t))$ is a source term. The Galilei Invariant advection-diffusion with a non linear source term is chosen as a second model given by

$$\frac{\partial u(x,t)}{\partial t} + \frac{\partial u(x,t)}{\partial x} = D_t^{1-\gamma(x,t)}\Big(\frac{\partial^2 u}{\partial x^2}\Big) + R(x,t,u), \tag{4.47}$$

with initial and boundary condition as

$$\begin{aligned} u(x,0) &= f_2(x), \\ u(0,t) &= g_3(t),, \\ u(1,t) &= g_4(t). \end{aligned} \tag{4.48}$$

This variable order advection diffusion model can present a more effective mathematical framework for description of different real world anomalous diffusion process.

4.7 Description of proposed method

In this section, Gegenbauer wavelet and their operational matrices are used to solve model (4.45) and (4.47). First, by approximating the unknown function $u(x,t)$ by Gegenbauer wavelet as

$$u(x,t) = \Psi(x)^T.U.\Psi(t), \tag{4.49}$$

Differentiating equation (4.49) with respect to x and t

$$\frac{\partial}{\partial x}u(x,t) = (\overline{D}.\Psi(x))^T.U.\Psi(t), \tag{4.50}$$

$$\frac{\partial}{\partial t}u(x,t) = \Psi(x)^T.U.\overline{D}.\Psi(t), \tag{4.51}$$

$$\frac{\partial^2}{\partial x^2}u(x,t) = \Psi(x)^T.U.\overline{D}^2.\Psi(t). \tag{4.52}$$

Applying variable order fractional derivative of order $\gamma(x,t)$ with respect to t in equation (4.49), we get

$${}_0D_t^{\gamma(x,t)}u(x,t) = \Psi(x)^T.U.Q_t^{\gamma(x,t)}.\Psi(t), \tag{4.53}$$

and also applying with respect to x, we obtain

$${}_0D_x^{\mu(x,t)}u(x,t) = (Q_x^{\mu(x,t)}.\Psi(x))^T.U.\Psi(t). \tag{4.54}$$

Putting the values of $u(x,t)$, $\frac{\partial}{\partial x}u(x,t)$, $\frac{\partial}{\partial t}u(x,t)$, $\frac{\partial^2}{\partial x^2}u(x,t)$,${}_0D_t^{\gamma(x,t)}u(x,t)$ from equations (4.49) $-$ (4.54) in given first model (4.45), the following is obtained as

$$\xi_1(x,t) = \Psi(x)^T.U.Q_t^{\gamma(x,t)}.\Psi(t) - (Q_x^{\mu(x,t)}\Psi(x))^T.U.\Psi(t) - \kappa(\Psi(x)^T.U.\Psi(t)) - f(x,t), \tag{4.55}$$

and substituting those in second model, we obtain

$$\begin{aligned}\xi_2(x,t) =&(\Psi(x))^T.U.\overline{D}.\Psi(t) + (\overline{D}.\Psi(x))^T.U.\Psi(t) - (\overline{D}^2\Psi(x))^T.U.Q_t^{1-\gamma(x,t)}.\Psi(t)\\ &- R(x,t,\Psi(x)^T.U.\Psi(t)).\end{aligned} \tag{4.56}$$

Using equation (4.49) into prescribed initial and boundary conditions given in equations (4.46), we get

$$\Psi(x)^T.U.\Psi(0) - f_1(x) = 0, \tag{4.57}$$

$$\Psi(0)^T.U.\Psi(t) - g_1(t) = 0, \tag{4.58}$$

$$\Psi(1)^T.U.\Psi(t) - g_2(t) = 0, \tag{4.59}$$

and from initial and boundary conditions given in equation (4.48), we obtain

$$\Psi(x)^T.U.\Psi(0) - f_2(x) = 0, \tag{4.60}$$

$$\Psi(0)^T.U.\Psi(t) - g_3(t) = 0, \tag{4.61}$$

$$\Psi(1)^T.U.\Psi(t) - g_4(t) = 0. \tag{4.62}$$

To obtain an approximate solution, the unknown matrix U is to be find out. The equations (4.55), (4.57) – (4.59) and (4.56), (4.60) – (4.62) are collocated for model 1 and model 2, respectively at points $x, t = 0, \frac{1}{\hat{m}}, \frac{2}{\hat{m}} \cdots, \frac{\hat{m}-1}{\hat{m}}$, and solving this nonlinear system of equations to find U. After finding U, the numerical solutions can be obtained for both the models upto desired degrees of accuracy.

4.8 Results and discussion

In this section the validity of the method is shown through applying it on various examples of both the types of models having exact solutions with prescribed initial and boundary conditions. All numerical computations are done using Wolfram Mathematica version-11.3.

TABLE 4.1: Variations of absolute error for different x at $t = 0.5$,$\lambda = 2$ and various $\hat{m}$.

$x \downarrow$	$\hat{m}$=4	$\hat{m}$=6	$\hat{m}$=8
0.2	3.2×10^{-14}	4.4×10^{-15}	1.88×10^{-15}
0.4	2.1×10^{-14}	1.7×10^{-15}	2.2×10^{-15}
0.6	1.2×10^{-14}	1.8×10^{-15}	3.1×10^{-15}
0.8	6.7×10^{-15}	2.2×10^{-15}	2.67×10^{-15}

TABLE 4.2: Comparison of absolute error for method given in [18] and the proposed method for different x at $t = 1$

x $\downarrow$	method in [18]	proposed method
0.2	5.9×10^{-5}	4.4×10^{-16}
0.3	8.8×10^{-5}	1.3×10^{-15}
0.4	1.1×10^{-4}	8.8×10^{-16}
0.6	1.3×10^{-4}	1.7×10^{-15}
0.7	1.2×10^{-4}	1.8×10^{-15}
0.8	1×10^{-4}	8.8×10^{-16}
0.9	5.6×10^{-5}	7.5×10^{-15}

Example 1:

Considering $\gamma(x,t) = \frac{2+\sin(xt)}{4}$, $f(x,t) = 20x^2(1-x)\left(\frac{t^{2-\gamma(x,t)}}{\Gamma(3-\gamma(x,t))} + \frac{t^{1-\gamma(x,t)}}{\Gamma(2-\gamma(x,t))}\right)$, $\kappa(u) = 0$ and $\mu(x,t) = 2$ so that the model (4.45) is reduced to

$$ {}_0D_t^{\gamma(x,t)} u(x,t) = \frac{\partial^2 u(x,t)}{\partial x^2} + f(x,t). \tag{4.63}$$

The equation (4.63) with the aid of initial and boundary conditions

$$ u(x,0) = 10x^2(1-x), u(0,t) = 0, u(1,t) = 0, \tag{4.64}$$

gives the exact solution as $u(x,t) = 10x^2(1-x)(t+1)^2$ [18].

The graphs of numerical and exact solutions for $\hat{m} = 4$ are shown through Figure 4.1. The absolute error for various $\hat{m}$ is shown in Table 4.1. The results clearly predict that our numerical results are in complete agreement with the existing results.

From Table 4.2, it is found that the error obtained by the proposed method is more

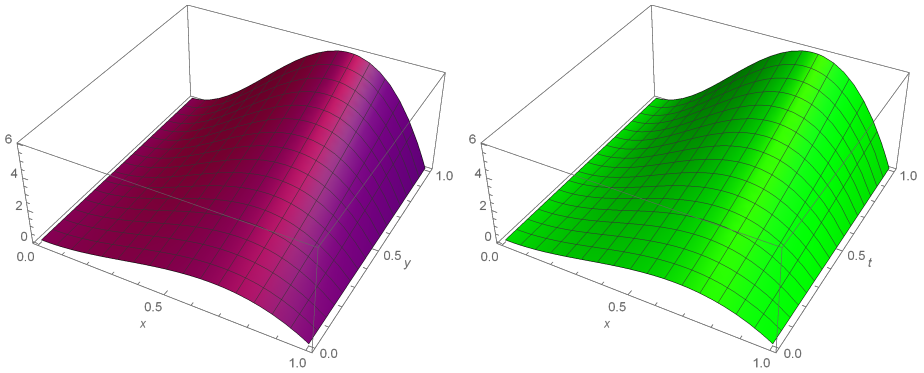

(a) Numerical solution (b) Exact solution

FIGURE 4.1: Plots of $u(x,t)$ for $\hat{m}=4$ and $\lambda=2$ in case of numerical and exact solution for $t=0.5$.

accurate as compared to the existing numerical method [18].

Example 2:

Considering $\gamma(x,t)=1$, $\mu(x,t)=\frac{6+xt}{4}$ so that proposed model (4.45) is reduced to

$$\frac{\partial u}{\partial t}-{}_0D_x^{\mu(x,t)}u(x,t)+x\sin u=f(x,t), \tag{4.65}$$

which under the prescribed initial and boundary conditions

$$u(x,0)=6, u(0,t)=6, u(1,t)=6+t, \tag{4.66}$$

gives the exact solution as $u(x,t)=(x^{3.2}-2x^{4.2}+x^{5.2})(t+t^2)+xt+6$ [19], by choosing the proper value of $f(x,t)$.

The absolute error for various $\hat{m}$ is shown in Table 4.3. The graphs of numerical and exact solutions for $\hat{m}=4$ are shown in Figure 4.2 which clearly predict that the obtained numerical results are in complete agreement with the existing results.

TABLE 4.3: Variations of absolute error for different x at $t = 0.5$, $\lambda = 2$ and various $\hat{m}$.

x ↓	$\hat{m}$=4	$\hat{m}$=6	$\hat{m}$=8
0.2	3.4×10^{-13}	2.6×10^{-14}	4.8×10^{-15}
0.4	9.7×10^{-13}	5.4×10^{-14}	4.0×10^{-15}
0.6	1.5×10^{-12}	7.7×10^{-14}	1.4×10^{-15}
0.8	2.1×10^{-12}	9.2×10^{-14}	2.4×10^{-15}

TABLE 4.4: Comparison of absolute error for method given in [19] and proposed method

(x,t) ↓	method given in [19]	proposed method
(0.1,0.1)	2.65×10^{-6}	2.1×10^{-15}
(0.3,0.3)	5.67×10^{-5}	2.4×10^{-15}
(0.5,0.5)	6.22×10^{-5}	2.9×10^{-15}
(0.7,0.7)	3.75×10^{-4}	7.4×10^{-15}
(0.9,0.9)	4.16×10^{-4}	9.9×10^{-15}

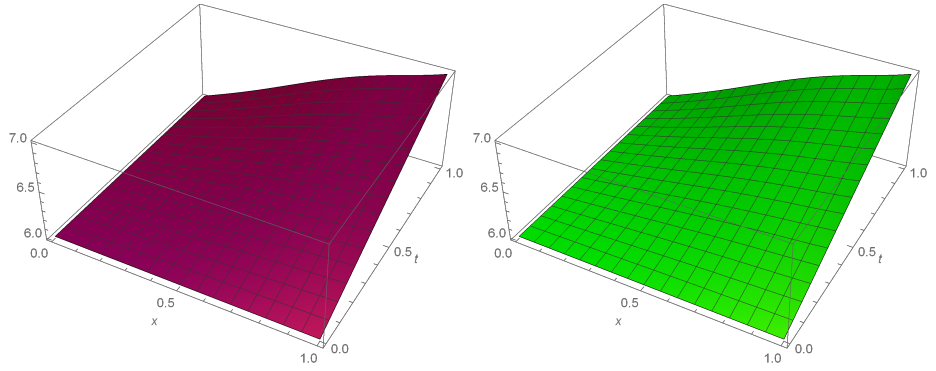

(a) Numerical solution (b) Exact solution

FIGURE 4.2: Plots of $u(x,t)$ for $\hat{m} = 4$ and $\lambda = 2$ in case of numerical and exact solution for $t = 0.5$.

Example 3:

Taking $\gamma(x,t) = \frac{2+\sin(t)}{400}$, $f(x,t) = \frac{\Gamma(\beta+1)}{\Gamma(\beta+1-\gamma(x,t))}$, $\kappa(u) = \frac{u}{4}$ and $\mu(x,t) = 2$ then proposed model (4.45) is reduced to

$$ {}_0D_t^{\gamma(x,t)} u(x,t) = \frac{\partial^2 u(x,t)}{\partial x^2} + \frac{u}{4} + f(x,t). \tag{4.67} $$

TABLE 4.5: Variations of absolute error for different x at $t = 0.5$, $\lambda = 2$ and various $\hat{m}$.

x ↓	$\hat{m}$=4	$\hat{m}$=6	$\hat{m}$=8
0.2	1.9×10^{-3}	2.8×10^{-5}	1.8×10^{-7}
0.4	1.6×10^{-3}	2.1×10^{-5}	1.5×10^{-7}
0.6	1.9×10^{-3}	2.3×10^{-5}	1.6×10^{-7}
0.8	2.6×10^{-3}	3.3×10^{-5}	2.2×10^{-7}

TABLE 4.6: comparison of L_∞ error for method given in [20] and proposed method

M ↓	method in[20]	proposed method
4	3.86×10^{-2}	2.8×10^{-3}
8	4.23×10^{-3}	3.1×10^{-7}

The equation (4.67) with initial and boundary conditions

$$u(x,0) = 0, u(0,t) = 0, u(1,t) = t^\beta, \tag{4.68}$$

gives the exact solution $u(x,t) = t^\beta \sin(\frac{x}{2})$ [20].

The graphs of numerical and exact solutions for $\hat{m} = 4$ are shown in Figure 4.3 and the absolute error is shown in Table 4.5. The results clearly predict that obtained numerical results are in complete agreement with the existing results. It is seen from the Table 4.6 that the proposed method is much superior as compared to the existing numerical method [20] when maximum absolute error is computed for the given example.

Example 4:

Taking $\gamma(x,t) = 2x$, $\kappa(u) = cu(1-\frac{u^3}{3})$ and $\mu(x,t) = 2t$, so that the following variable order space and time both fractional problem is obtained as

$${}_0D_t^{2x}u(x,t) = {}_0D_x^{2t}u(x,t) + cu(1 - \frac{u^3}{3}) + f(x,t), \tag{4.69}$$

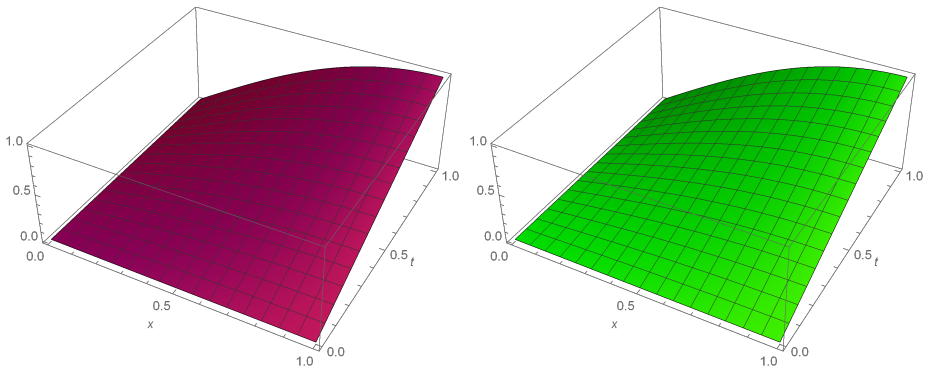

(a) Numerical solution (b) Exact solution

FIGURE 4.3: Plots of $u(x,t)$ for $\hat{m}=4$ and $\lambda=2$ in case of numerical and exact solution for $t=0.5$.

TABLE 4.7: Variations of absolute error for different x at $t=0.5$, $\lambda=2$ and various $\hat{m}$.

x $\downarrow$	$\hat{m}$=4	$\hat{m}$=6	$\hat{m}$=8
0.2	1.7×10^{-6}	1.2×10^{-10}	1.3×10^{-12}
0.4	5.8×10^{-6}	4.9×10^{-10}	4.9×10^{-12}
0.6	1×10^{-5}	9.7×10^{-9}	9.5×10^{-11}
0.8	1.4×10^{-5}	1.4×10^{-9}	1.8×10^{-11}

under the initial and boundary condition as

$$u(x,0)=0, \tag{4.70}$$

$$u(0,t)=0, \tag{4.71}$$

$$u(1,t)=t, \tag{4.72}$$

and $f(x,t)$ is chosen such that the exact solution of above the problem is obtained as $u(x,t)=xt$. The graphs of numerical and exact solutions for $\hat{m}=4$ are shown in Figure 4.4. The results of absolute error given in Table 4.7 clearly predict the error between the numerical solution and the exact solution decreases as the degree of approximation increases. The VORDE characterizes the behavior of reaction and diffusion of pollute in groundwater. Here it is assumed that the concentration of pollute is zero at time $t=0$. At the initial boundary $x=0$, the concentration

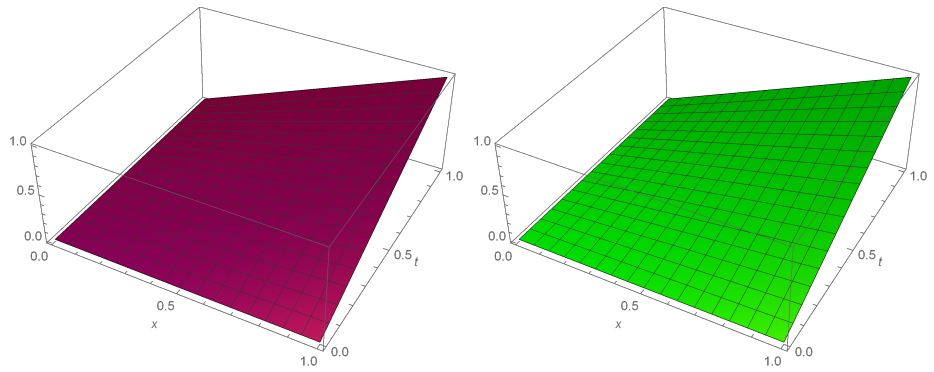

(a) Numerical solution (b) Exact solution

FIGURE 4.4: Plots of $u(x,t)$ for $\hat{m}=4$ and $\lambda=2$ in case of numerical and exact solution for $t=0.5$.

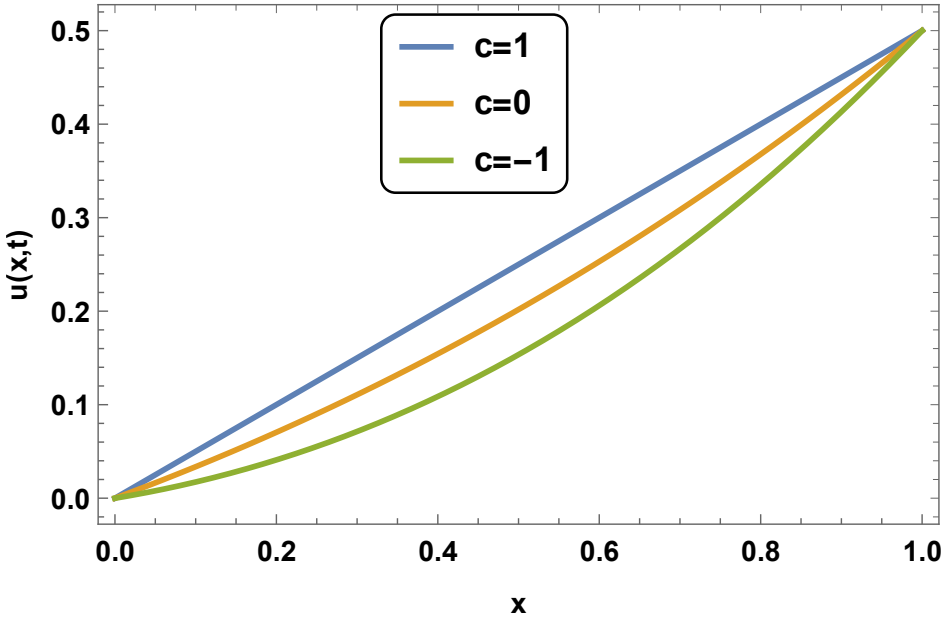

FIGURE 4.5: Behavior of $u(x,t)$ for $\hat{m}=4$ and $\lambda=2$ at $t=0.5$.

of pollute is zero and increases linearly towards the boundary $x=1$. From Figure 4.5 the case $c=0$ represents when pollute has no reaction with groundwater. While the cases $c=1$ (source term) and $c=-1$ (sink term) represent the cases when it is reacting with groundwater. It is observed that in case of $c=1$, the concentration of pollute is more than when the pollute has no reaction with groundwater while in case of $c=-1$ behavior of solution is opposite. Figure 4.5 also shows that

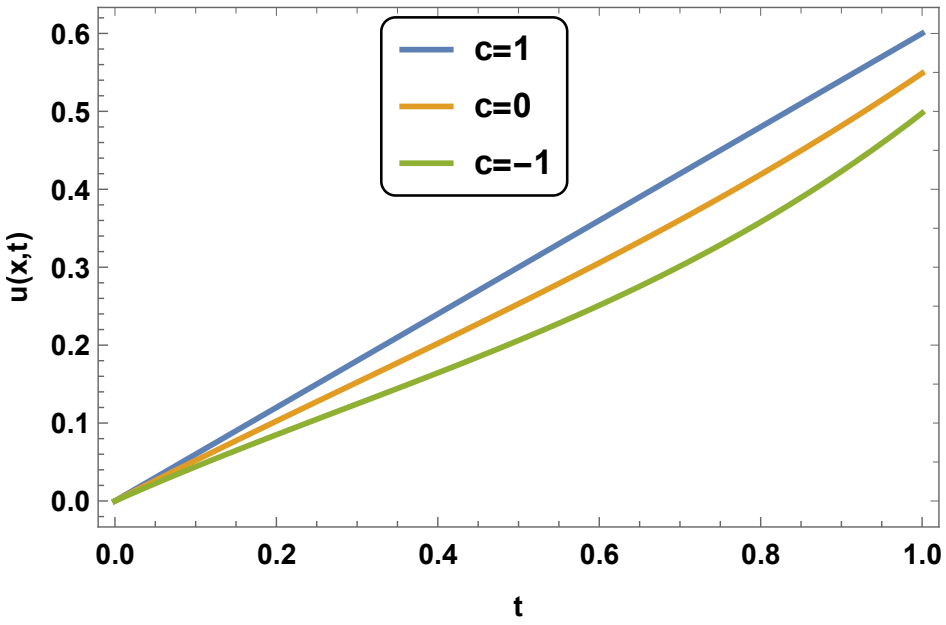

FIGURE 4.6: Behaviour of $u(x,t)$ for $\hat{m}=4$ and $\lambda=2$ at $x=0.5$.

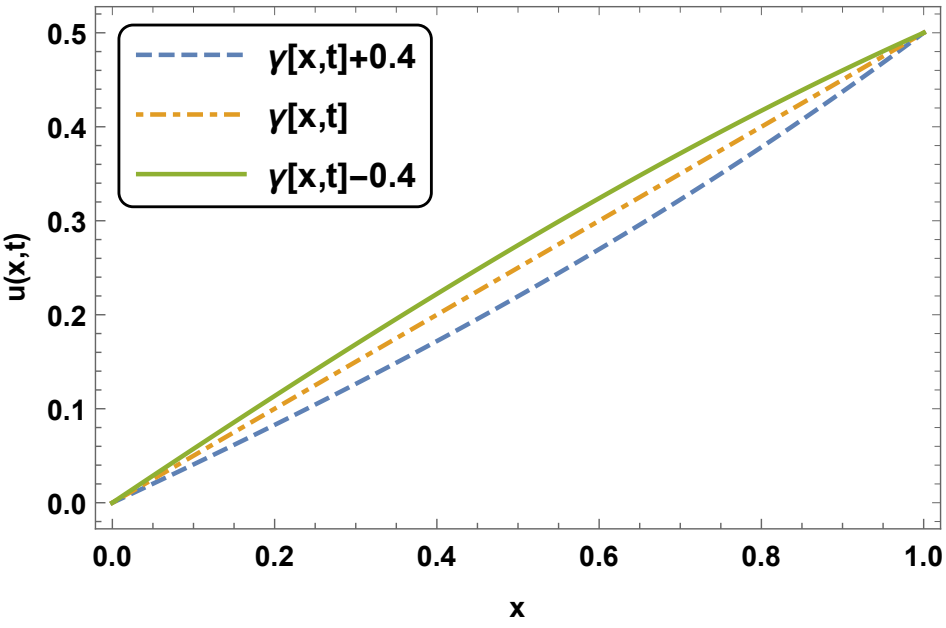

FIGURE 4.7: Behaviour of $u(x,t)$ for $\hat{m}=4$ and $\lambda=2$ at $x=0.5$.

concentration decreases at invasive fronts of site. Figure 4.6 depicts that at time $t=0$, the concentration is zero and its growth increases with time.

Figure 4.7 depicts the fact that pollute concentration decreases when an accession is added to the variable order exponent of time $\gamma(x,t)$ while concentration is more

TABLE 4.8: Variations of absolute error for different x at $t = 0.5$, $\lambda = 2$ and various $\hat{m}$.

x ↓	$\hat{m}$=4	$\hat{m}$=6	$\hat{m}$=8
0.2	5.7×10^{-4}	3.3×10^{-6}	9.1×10^{-9}
0.4	5.6×10^{-4}	3.2×10^{-6}	8.8×10^{-9}
0.6	5.8×10^{-4}	3.3×10^{-6}	9.1×10^{-9}
0.8	6.4×10^{-4}	3.6×10^{-6}	9.6×10^{-9}

if a shrinkage is given of amount 0.4 to $\gamma(x,t)$. It also shows that this growth and reduction of concentration are higher around the middle of site as compared to invasive fronts.

Example 5:

Taking $\gamma(x,t) = \frac{10-tx}{300}$, $R(x,t,u) = u - u^2 + e^x t\Big(2 + e^x t^3 - 2\frac{t^{\gamma(x,t)}}{\Gamma(2+\gamma(x,t))}\Big)$, our model (4.47) is reduced to

$$\frac{\partial u(x,t)}{\partial t} + \frac{\partial u(x,t)}{\partial x} = D_t^{1-\gamma(x,t)}\Big(\frac{\partial^2 u}{\partial x^2}\Big) + R(x,t,u), \tag{4.73}$$

which with the aid of initial and boundary conditions as

$$u(x,0) = 0, u(0,t) = t^2, u(1,t) = et^2, \tag{4.74}$$

gives the exact solution as $u(x,t) = t^2 e^x$ [99].

The graphs of numerical and exact solutions for $\hat{m} = 4$ are shown in Figure 4.7. Here the absolute error decreases steadily as the degree of approximation increases. The results clearly predict that obtained numerical results are in complete agreement with the existing results.

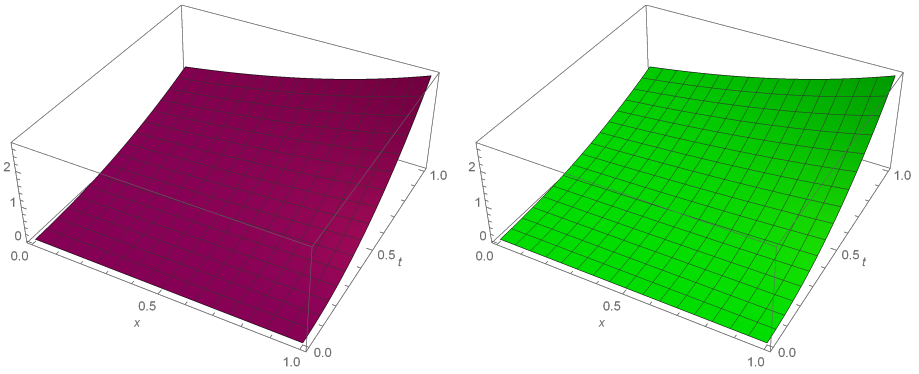

(a) Numerical solution (b) Exact solution

FIGURE 4.8: Plots of $u(x,t)$ for $\hat{m}=4$ and $\lambda=2$ in case of numerical and exact solution for $t=0.5$.

Example 6:

The model (4.47) with $\gamma(x,t) = \frac{1}{500}\big((tx)^2 - \sin^3 tx + cos^4 tx + 266\big)$, $R(x,t,u) = u - u^2 + te^{-}2x\Big(t^3 - 2(t-1)e^x - \frac{2e^x t^{\gamma(x,t)}}{\Gamma(2+\gamma(x,t))}\Big)$ is reduced to

$$\frac{\partial u(x,t)}{\partial t} + \frac{\partial u(x,t)}{\partial x} = D_t^{1-\gamma(x,t)}\Big(\frac{\partial^2 u}{\partial x^2}\Big) + R(x,t,u), \tag{4.75}$$

The equation (4.75) with initial and boundary conditions as

$$u(x,0) = 0, u(0,t) = t^2, u(1,t) = e^{-1}t^2, \tag{4.76}$$

give the exact solution as $u(x,t) = t^2 e^{-x}$ [99].

The graphs of numerical and exact solutions for $\hat{m}=4$ are shown in Figure 4.8. The results clearly predict that obtained numerical results are in complete agreement with the existing results. The absolute error between exact and numerical solution is given in Table 4.9.

TABLE 4.9: Variations of absolute error for different x at $t = 0.5$, $\lambda = 2$ and various $\hat{m}$.

x ↓	$\hat{m}$=4	$\hat{m}$=6	$\hat{m}$=8
0.2	2.3×10^{-4}	1.2×10^{-6}	3.4×10^{-9}
0.4	2.1×10^{-4}	1.1×10^{-6}	3.0×10^{-9}
0.6	1.9×10^{-4}	1×10^{-6}	2.9×10^{-9}
0.8	1.9×10^{-4}	1.1×10^{-6}	3×10^{-9}

4.9 Conclusion

In this chapter, the four important consequences have been achieved. First one, the operational matrix for variable order is derived. Second one, the successful implementation of collocation method based on Gegenbauer wavelets to solve the variable order non linear reaction-diffusion equation and non-linear Galilei-invariant advection diffusion equation. Third one is finding the error bound and stability analysis of the proposed method. The last one is the graphical and tabular exhibitions to validate the effectiveness of the proposed method used for solving various linear/nonlinear problems derived from two considered mathematical models for different particular cases. The beauty of the present contribution is the showering of the effect of reaction term on the solute concentration for different particular cases.

****